Reliable and Efficient Electrochemical Recovery of O_2 from Metabolic CO_2 at the International Space Station (ISS)

Jesus A. Dominguez,
Insight Global/Jacobs Space Exploration Group (JSEG), Huntsville, AL, 35806

Lorlyn Reidy, Mononita Nur, Kagen Crawford, Brittany Brown
NASA Marshall Space Flight Center, Huntsville, Alabama, 35811

Brian Dennis, Wilaiwan Chanmanee
University of Texas at Arlington, Arlington, Texas, 76019

Joseph Fillion, Kathryn Ollenburg
Jacobs Space Exploration Group (JSEG), Huntsville, AL, 35806

Shannon McCall
Qualis Corporation /Jacobs Space Exploration Group (JSEG), Huntsville, AL, 35806

Maximum O_2 recovery from metabolic carbon dioxide (CO_2) is desired for future long-duration missions beyond Low Earth Orbit (LEO). The O_2 recovery for the Environmental Control and Life Support System (ECLSS) at the International Space Station (ISS), presently limited to 50% (Sabatier), must be highly reliable and efficient and recover a minimum of 75% oxygen (O_2) from metabolic CO_2. An alternative technology development effort currently underway at NASA Marshall Space Flight Center (MSFC) via a Macrofluidic Electrochemical Reactor (MFECR) approach has the potential to increase O_2 recovery significantly and reduce the complexity of the ECLSS O_2 recovery at the ISS as it would replace three pieces, the CO_2 Reduction Assembly (CRA) (Sabatier reactor), the Oxygen Generation Assembly (OGA), and the Plasma Pyrolysis Assembly (PPA). The MFECR's electrochemical process generates ethylene (C_2H_4) and carbon monoxide (CO) instead of methane (CH_4) (Sabatier) as a byproduct, eliminating the need for further dehydrogenation through the PPA. As in the OGA, the MFECR's electrochemical process generates O_2 and hydrogen (H_2) from the water electrolysis process. MSFC and the University of Texas in Arlington (UTA) have jointly designed and fabricated/upgraded an MFECR's single cell that operates at ambient conditions and utilizes a proprietary catalyst highly selective on reducing CO_2 to C_2H_4 and CO at the cathode. This MFECR's single cell consists of gas diffusion layers at the cathode and anode for respective intake of CO_2 and output of O_2 from the catalytic layer. This approach is expected to substantially improve the ISS ECLSS sustainability and reduce power and weight requirements as the MFECR would replace three and potentially four units currently installed in the ISS. In this paper, the authors discuss the outcome of preliminary tests, the current development, the evaluation efforts on different alternatives for the cathode and the anode configurations, the use of MFECR's digital twin to upgrade its design at an engineering development unit (EDU) scale, and the evaluation efforts on different electrolyte alternatives and alkalinity effect.

Nomenclature

AC	=	Activated carbon
AR	=	Atmospheric revitalization
AHA	=	Aprotic heterocyclic anions
BPC	=	Back pressure controller
BZY	=	Yttria-doped Barium Zirconate
CDRA	=	Carbon dioxide removal assembly
CRA	=	Carbon dioxide reduction assembly
CO2R	=	Carbon dioxide reduction
CO_2	=	Carbon dioxide
C_2H_4	=	Ethylene

C_2H_2 = Acetylene
CH_4 = Methane
CL = Catalyst layer
EC = Electrochemical
ECRe = Electrolytic O_2 Recovery
EDU = Engineering design unit
ECLSS = Environmental Control and Life Support System
GC = Gas chromatography
GDL = Gas diffusion layer
GDE = Gas diffusion electrode
IL = Ionic liquid
HER = Hydrogen evolution reaction
KOH = Potassium hydroxide
LEO = Low Earth Orbit
MEA = Membrane electrode assembly
MFECR = Macro-fluidic electrochemical reactor
MPL = Macropore layer
MSFC = Marshall Space Flight Center
NASA = National Aeronautics and Space Administration
N_2 = Nitrogen
Ni = Nickel
OER = Oxygen evolution reaction
OGA = Oxygen generation assembly
O_2 = Oxygen
OH^- = Hydroxide ion
pKa = Acid-ionization constant
SOA = State-of-the-art
SOEC = Solid oxide electrochemical cell
Pt = Platinum
PPA = Plasma pyrolysis assembly
PTFE = Poly-tetra-fluoro-ethylene
H_2 = Hydrogen
ISS = International Space Station
SEM/EDX= Scanning electron microscopy-energy dispersive X-ray
SSRS = Solid-state reactive sintering
UTA = University of Texas at Arlington

I. Introduction

To sustainably recover O_2 from metabolic CO_2, we will need to:

1) Replicate and reverse the metabolic energy production in the human body that yields 1 kg per day of metabolic CO_2 and water from the carbohydrate intake with an H/C ratio of 1.8.
2) Yield C_nH_m byproducts with m/n < 2, preferably C_2H_4 or C_2H_2, as their H/C ratios are 2 and 1, respectively, to sustain a closed-loop atmospheric revitalization (AR) and allow their disposal without affecting the closed-loop of the AR system, otherwise, water loss needs to be constantly restituted to keep CO_2 reduction (CO_2R) operating.
3) Minimize the generation of CO, a byproduct in most O_2 recovery processes, to achieve a theoretical O_2 recovery higher than 50%.

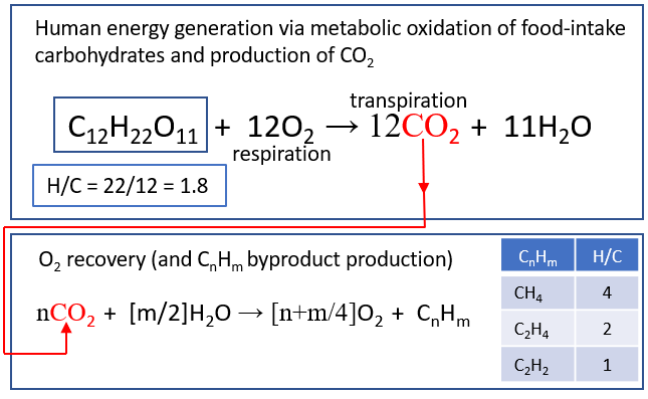

Figure 1. Generation of metabolic CO_2 and the corresponding O_2 recovery.

Figure 1 illustrates how the human body generates and expels via transpiration 1 kg of metabolic CO_2 daily from two intakes (carbohydrates from solid food and O_2 from respiration/breathing air) and the respective recovery of the O_2 along with the generation of C_nH_m byproduct. The sustainable H/C input ratio of 1.8 is far lower than the 4:1 ratio of methane, which is the product of the Sabatier process currently used in the metabolic O_2 recovery system at the International Space Station (ISS).

The current O_2 recovery from metabolic CO_2 at the ECLSS requires four interconnected units, as shown in Figure 2: the carbon dioxide removal assembly (CDRA), the carbon dioxide reduction assembly (CRA), the oxygen generation assembly (OGA), and the plasma pyrolysis assembly (PPA). The CDRA (packed bed adsorber) takes the air and removes the metabolic CO_2 from the air, which is returned to the cabin; the CRA (Sabatier reactor) takes the CO_2 from the CDRA and hydrogen (H_2) from the OGA (water electrolyzer) and produces water (H_2O) and methane (CH_4) recovering approximately 50% of O_2 from metabolic CO_2. The reaction that takes place in the Sabatier reactor is illustrated in Equation 1; the H_2O is fed to the OGA to produce O_2 and H_2 via H_2O electrolysis, as described in Equation 2; the CH_4 from the Sabatier reactor is dehydrogenated at the PPA that uses a magnetron to generate an H_2/CH_4 plasma that converts the CH_4 generated from Sabatier into mainly H_2 and C_2H_2 as shown in Equation 3; the H_2 from two sources, the OGA and the separation unit connected to the PPA, is recycled back to the CRA and the O_2 is released into the cabin for crew consumption. The global reaction leads to the recovery of O_2 from CO_2 in the form of water, as illustrated in Equation 4.

Sabatier:	$2CO_2 + 8H_2 \leftrightarrow 4H_2O + 2CH_4$	(1)
Water Electrolysis:	$2H_2O \rightarrow 2H_2 + O_2$	(2)
PPA:	$2CH_4 \leftrightarrow 3H_2 + C_2H_2$	(3)
Total:	$2CO_2 + 3H_2 \rightarrow C_2H_2 + 2H_2O + O_2$	(4)

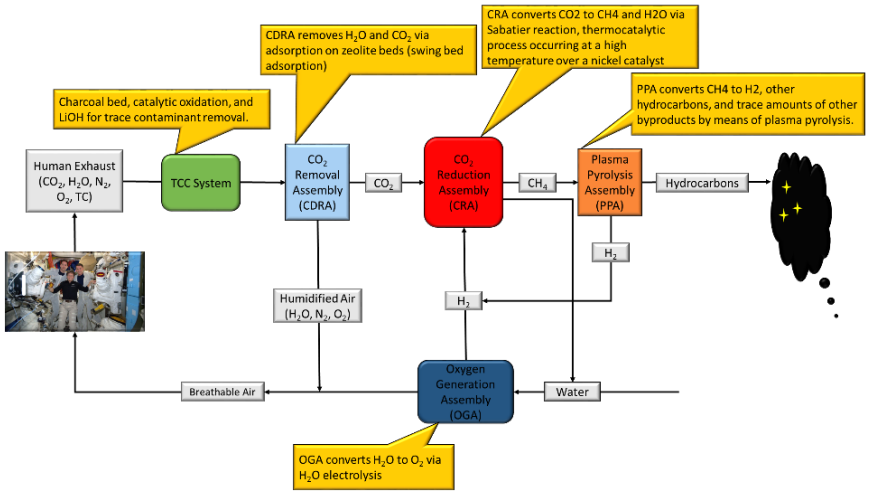

Figure 2. Current SOA O_2 recovery onboard ISS with the addition of PPA.

Although Sabatier/PPA technology is the current baseline exploration O_2 recovery architecture, alternative approaches, such as the electrolytic reduction of CO_2, may be more desirable for future long-duration missions, as maximum O_2 recovery from metabolic CO_2 and lower H_m/C_n ratio byproduct are desired for future long-duration missions beyond low earth orbit (LEO). Daily metabolic generation of 1 kg of CO_2 is associated with carbohydrate intake with an H/C ratio of 1.8.

In 2016, NASA's Game Changing Development Program awarded the University of Texas Arlington (UTA) a contract to develop a MFECR that uses copper-bromine electrocatalysis developed by UTA researchers[1,2,3] that reduces CO_2 selectively to C_2H_4 over CO and CH_4, standard products from similar electrochemical (EC) reduction of CO_2 using copper-based electrocatalysis at ambient conditions. CO and CH_4 are more undesired byproducts than C_2H_4 as the formation of CO reduces O_2 recovery, and the formation of CH_4 consumes more water than the formation of C_2H_4 since it has a lower H/C ratio,

C_2H_4 is a more desirable byproduct than CH_4 generated by the Sabatier reactor as the H/C ratio of C_2H_4 (2) is half of the H/C ratio of CH_4 (4) and closer to 1.8 (carbohydrate intake), indicating that C_2H_4 carries lower water loss than CH_4 as the H_2 source on both byproducts is H_2O present in the aqueous solution.

The architecture of an Electrolytic O_2 Recovery (EORe) system coupled with an MFECR is shown in Figure 3. The EORe System would reduce complexity by eliminating CRA, PPA, and OGA. The current CRA and other technologies that are being investigated (i.e., PPA and Bosch technologies) operate at extremely high temperatures resulting in heavy reactors and higher power consumption, making the MFECR highly attractive for future exploration missions.

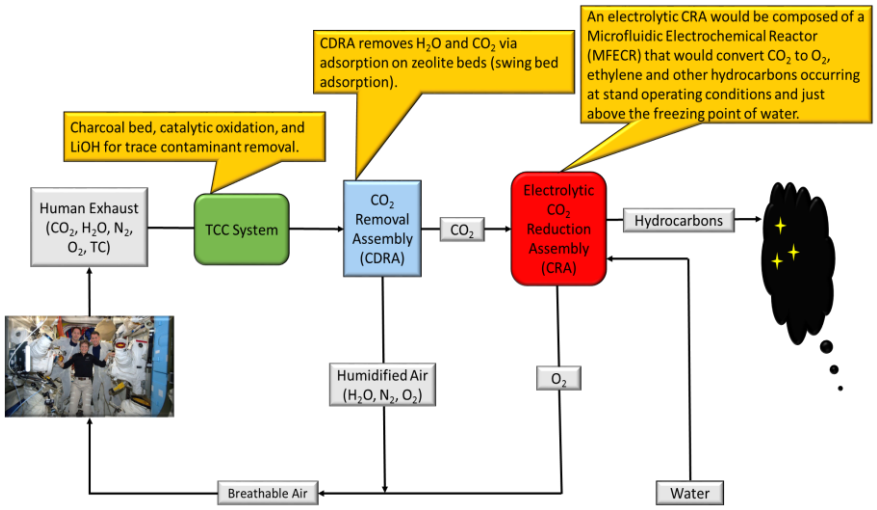

Figure 3. O_2 recovery system for future long duration missions utilizing electrolytic technology, which eliminates the need for OGA, Sabatier, and PPA

MFECR can potentially replace CRA and OGA as it performs both functions in a single unit: EC reduction of CO_2 to O_2 (CRA) and generation of O_2 and H_2 via electrolysis (OGA). MFECR's carbon-based byproduct, C_2H_4, does not require further dehydrogenation as in the Sabatier reactor yielding CH_4, eliminating the need for the third unit, the PPA. The MFECR approach can potentially go further and eliminate the need for the CDRA; as illustrated in Figure 4, the air might directly be fed to a set of MFECRs, skipping the CDRA.

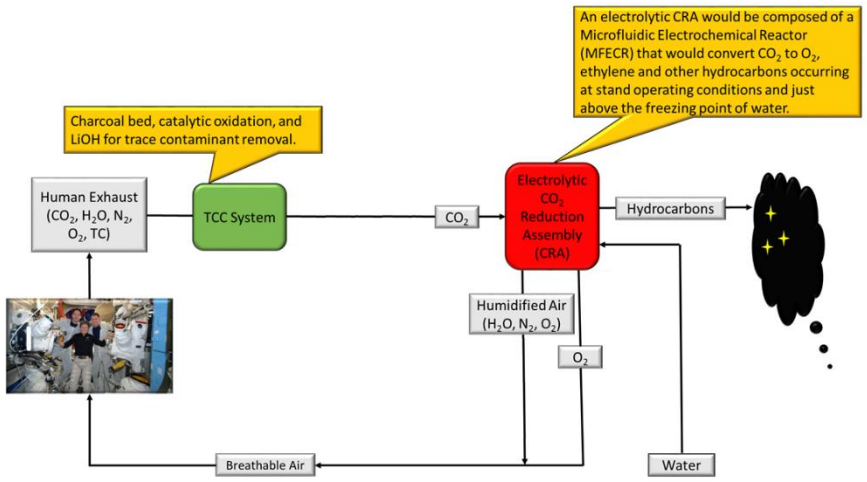

Figure 4. O_2 recovery system for future long duration missions utilizing electrolytic technology skipping prior CO_2 removal from air, which eliminates the need for OGA, Sabatier, PPA, and CDRA.

A digital twin (replica) of the MFECR single cell built/deployed via a comprehensive 3D model was used to theoretically assess the O_2 recovery from CO_2 using 3,000–6,500 ppm of metabolic CO_2 in air (breathing concentration aboard the ISS) instead of 100% (concentration currently obtained from the CDRA after the removal of 3,000–6,500 ppm of metabolic CO_2 from the air). The theoretical evaluation shows that a stack of MFECRs can handle direct air feed with 3,000–6,500 ppm of metabolic CO_2 and obtain equivalent O_2 recovery than a smaller stack of MFECRs

handling 100% CO_2 from the CDRA. It might be considered the absorption of two additional gases, O_2 and N_2, in the alkaline electrolyte solution. O_2 and N_2 have a lower solubility in water than CO_2; the solubility of O_2 in water at ambient conditions is 1.38E-3 M, and that of N_2 is 0.69E-3 M, while the solubility of CO_2 in water is 3.8E-2 M.

Figure 5 shows a) a schematic of a cross-section of the MFECR single cell, b) an image of the MFECR cell mounted in the test stand and currently being used, and c) a general schematic of the H_2 separation approach and recovery of H_2O consumed in the MFECR. The MFECR cell consists of three channels. The two gas channels (anode and cathode) and the electrolyte channel are separated by a Gas Diffusion Electrode (GDE). The GDE has two embedded layers, the Gas Diffusion Layer (GDL) and the Macropore Layer (MPL), having different degrees of porosity and hydrophobic coating to manage the gas and liquid phases that meet on the Catalyst Layer (CL) formed on the MPL by electrodeposited nanocomposite particles that act as electrocatalysts on the cathode (copper-bromine nanocomposite) and anode (platinum nanocomposite). The electrolyte is an alkaline solution; Potassium hydroxide (KOH) is not consumed and must not be replaced. However, H_2O is depleted to yield O_2 and the byproducts C_2H_4, CO, and H_2, as illustrated in Equations 5, 6, and 7. It needs to be added to the KOH solution to replace the consumed H_2O and keep the KOH at the desired pH/concentration.

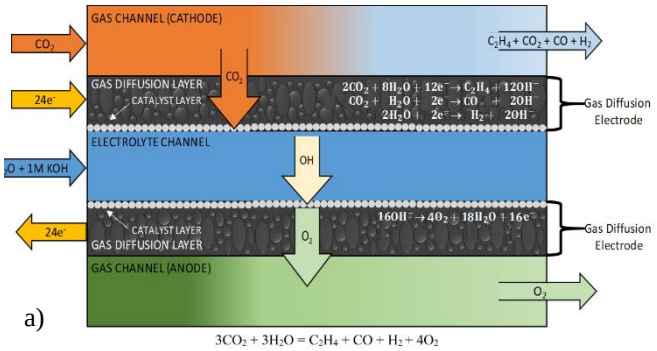

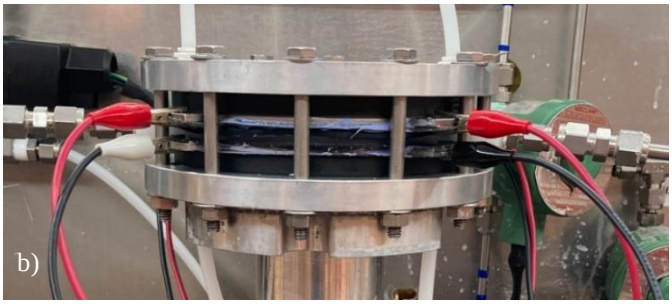

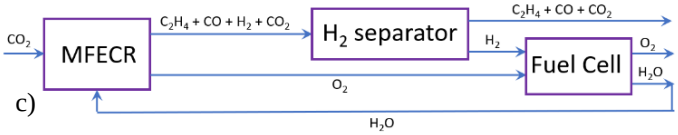

Figure 5. a) Schematic of cross section of the MFECR cell, b) Image of MFECR's EDU mounted in the test stand, c) General schematic of the H_2 separation approach and recovery of H_2O consumed in the MFECR.

Cathode

$2CO_2 + 8H_2O + 12e^- = C_2H_4 + 12OH^-$ (5)

$CO_2 + H_2O + 2e^- = CO + 2OH^-$ (6)

$2H_2O + 2e^- = H_2 + 2OH^-$ (7)

Anode

$16OH^- = 4O_2 + 8H_2O + 16e^-$ (8)

Total

$3CO_2 + 3H_2O = C_2H_4 + CO + H_2 + 4O_2$ (9)

In the cathode, three reactions are expected and have been observed to occur: the reduction of CO_2 to C_2H_4 and CO and the generation of H_2 from water (equations 5, 6, and 7, respectively). All three reactions generate hydroxide ions (OH^-). OH^- is generated at the cathode and then transported by the electrical potential applied to the MFECR cell through the electrolyte to the anode, consumed to produce O_2 and H_2O, as described in equation 8. During the process, O_2 and a mixture of H_2, C_2H_4, and CO are generated on separated MFECR cell sides (the cathode and the anode sides), which allows the regeneration of H_2O after feeding a fuel cell with the O_2 generated at the anode and H_2 generated at the cathode and separated from C_2H_4 and CO.

The test stand, shown in Figure 6, houses an MFECR EDU equipped with an electrolytic cell fed with CO_2 into the cathode gas channel, N_2 into the anode gas channel, and an electrolyte solution into the electrolyte channel. Mass flow controllers upstream of the cell control the cathode (CO_2) and anode (N_2) feed streams. Back Pressure Controllers (BPCs) measure the flow and control the anode and cathode outlet pressures. Both anode and cathode outlet streams are fed into a condenser to remove any condensation before entering the BPCs and prevent any damage to the BPCs and other components downstream. The electrical power utilized by the EDU's electrolytic cell is provided by a DC power supplier directly attached to the cell's anode and cathode contacts. The alkaline electrolyte solution continuously flows in a loop driven by a peristaltic pump, passing through a chiller before getting into the MFECR to set the inlet temperature; all the lines in the electrolyte-flow loop are wrapped with insulation. Further insulation work will be required on the MFECR and the electrolyte reservoir tank.

A gas chromatograph (GC) samples the inlet/outlet anode or cathode streams to measure the amount of C_2H_4, CO, and H_2 produced in the cathode channel and O_2 produced in the anode channel to determine the chemical conversion achieved by the electrolytic cell. Besides C_2H_4, CO, H_2, O_2, N_2, and CO_2 components, the GC has been calibrated to

detect and measure unexpected components, such as C_2H_2 and CH_4, in contrast with CH_4, C_2H_2, is an unforeseen desirable component as its H/C ratio is 1, lower than the water closed-loop threshold value of 1.8 imposed by the carbohydrate intake.

UTA and NASA MSFC collaborative efforts are underway to increase the O_2 recovery efficiency of the process to >50%, advance the technology readiness of the proposed technology to Technology Readiness Level (TRL) 4, and mature the hardware system to process 1.0 kg/day of CO_2. To achieve these goals, we are currently evaluating and developing efforts on different alternatives on not only the configuration and setup of the MFECR at an Engineering Design Unit (EDU) scale but also the selection of component materials.

Figure 6. Test stand at MSFC housing a MFECR at EDU scale.

II. Anode Composite Development

While for the cathode, commercially available GDEs are used with catalyst electrochemically deposited on the MPL side of the GDE forming the CL, the anode cannot utilize these carbon-based GDEs as they undergo carbonization with the O_2 generated at the anode. A GDE anode composite was fabricated in-house using a Nickel foam sandwiched between a poly-tetra-fluoro-ethylene (PTFE) film and a Nylon membrane[3], as illustrated in Figure 7. Two Nickel foam types, anodized and platinized, were tested. The PTFE film is in contact with the CO_2 gas phase and serves as a GDL for the CO_2 to reach the catalyst surface deposited on the anodized/platinized Nickel foam; the Nylon membrane is in contact with the aqueous electrolyte and serves as a mild hydrophobic layer to allow controlled contact of the electrolyte to the catalyst surface deposited on the anodized/platinized Nickel foam.

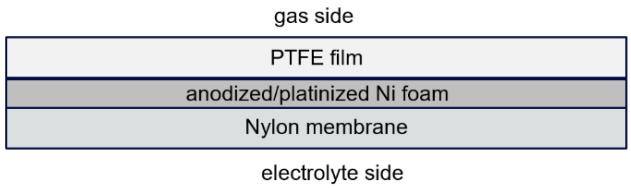

Figure 7. PTFE/Nickel/Nylon anode composite

Potassium carbonate (K_2CO_3) formation and precipitation were observed and verified via Scanning Electron Microscopy-energy Dispersive X-ray (SEM/EDX) analysis on anodized and platinized Nickel foams using 1 M KOH electrolyte at 2-5 Volts. As CO_2 is absorbed in the 1-M KOH solution, a fraction of the absorbed CO_2 decomposes to CO_3^{2-} anion, which reacts with the Potassium cation (K^+) dissolved in the solution to form and precipitate K_2CO_3.

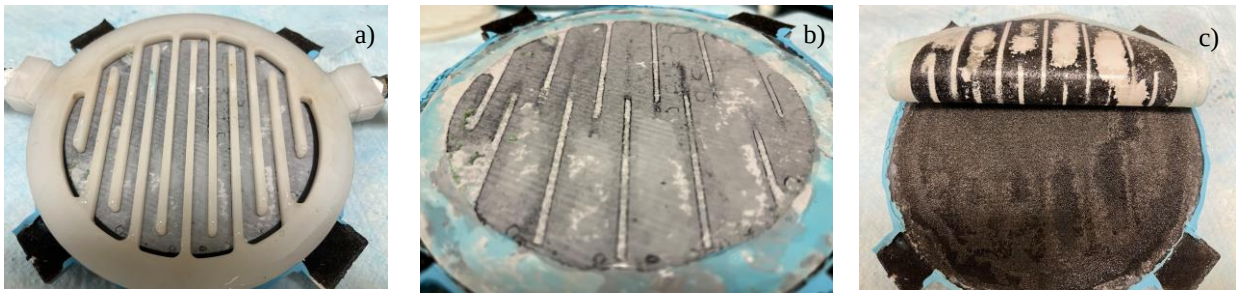

Figure 8. Potassium carbonate formation and precipitation on platinized Nickel foam anode in a test performed with 1 M KOH electrolyte at 3 Volts. a) electrolyte serpentine chamber with Nylon membrane on the bottom, b) Nylon membrane on electrolyte side after removing electrolyte serpentine chamber, c) Platinized Nickel foam and attached Nylon membrane.

Figure 8 depicts the Potassium carbonate (black solid) precipitated on the top side of the Nylon membrane throughout the electrolyte serpentine channel path (Figures 8a and 8b) and on the platinized Nickel foam and attached Nylon membrane (Figure 8c).

Nickel foam was no longer an option as an anode despite its desirable EC properties as an electrode due to the Potassium carbonate's induced formation and precipitation, maybe due to the Nickel catalytic effect, as illustrated in Figure 8. A Platinized Ti screen was used to replace the Nickel foam and sandwiched between the PTFE film and the Nylon membrane, as shown in Figure 9. Tests were performed using the same conditions for anodized/platinized Nickel foam (1 M KOH electrolyte at 2-5 Volts). No formation and precipitation of Potassium carbonate was observed, as illustrated in Figure 10.

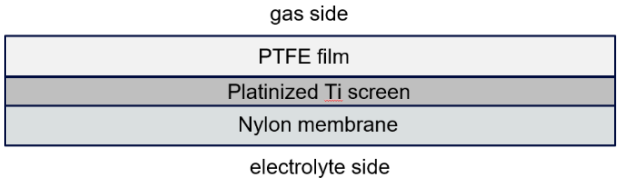

Figure 9. PTFE/Platinized Titanium/Nylon anode composite

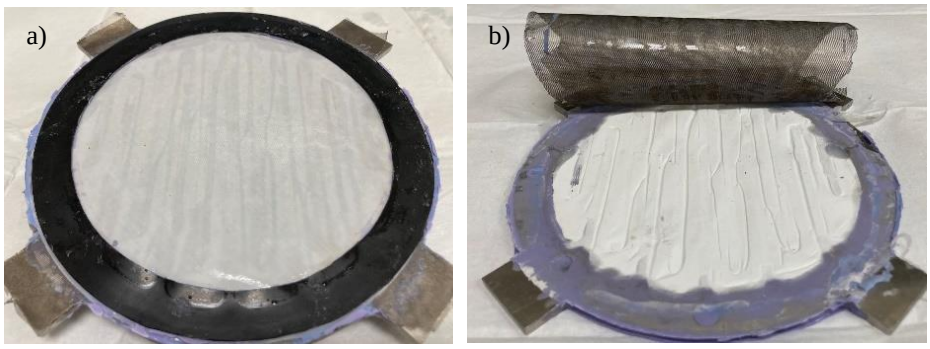

Figure 10. No formation and precipitation of potassium carbonate on platinized Titanium mesh anode in a test performed with 1 M KOH electrolyte at 3 Volts. a) Nylon membrane on electrolyte side after removing electrolyte serpentine chamber, b) Unfolded platinized Titanium mesh and attached Nylon membrane.

III. Preliminary Test Outcome

A. Electrolyte Temperature Effect

The temperature of the electrolyte plays a crucial role in the aqueous electrolysis of CO_2 as its absorption in the alkaline electrolyte solution increases at a lower temperature, dissolving more CO_2 gas and increasing its availability on the catalyst surface wetted by the electrolyte solution. A side effect of temperature decrement on the electrolyte solution is reduced electrical conductivity, which decreases at lower temperatures, in contrast with the CO_2 absorption. The significant gain in CO_2 solubility by reducing the inlet temperature superseded the decrement of electrical conductivity in the electrolyte, leading to an increment in O_2 recovery.

Cell Type	With serpentine
GDE	Sigracet 28 BC
GDE type	Modified with carbon black
GDE's cathode	Cu/Br (UTA)
GDE's anode	Platinized Ti PTFE/Pt-Ti/Nylon (UTA)
Ionomer on cathode	Fumasep 30 um
Ionomer on anode	None
A(cm^2)	72
Electrolyte	1 M KOH solution
CO_2 inlet flow (sccm)	50
N_2 inlet flow (sccm)	50
Electrolyte inlet flow (ml/min)	100
Potential (V)	3.5
Electrolyte temperature (C)	22 and 8

Table 1. EC cell setup with serpentine and operation conditions to assess the effect of electrolyte temperature and cell configuration on O_2 recovery from CO_2.

Table 1 lists the MFECR's EC cell and operation conditions used to evaluate the effect of temperature on the O_2 recovery from CO_2. The anode used was the composite one shown in Figure 9 with platinized Titanium sandwiched between PTFE film and Nylon membrane. The cathode used was the GDE Sigracet 28 BC modified with black carbon and with UTA's Cu-Br catalyst electrochemically deposited on the MPL of the GDE. Both inlet gas flow rates, CO_2 to the cathode and N_2 to the anode, were set to 50 sccm while the electrolyte flow rate was set to 100 ml/min. At the same potential of 3.5 V, two tests were performed with the electrolyte at 22 and 8 degrees Celsius, respectively.

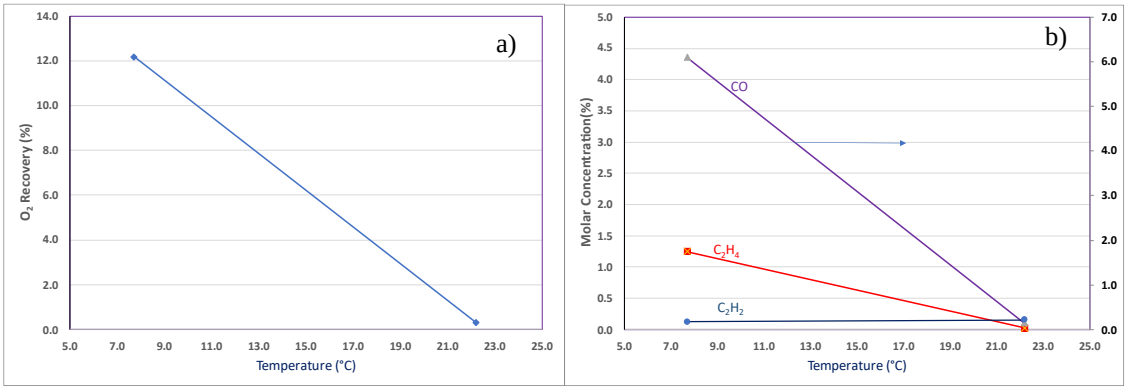

Figure 11. Effect of electrolyte temperature on O_2 recovery from CO_2 at 3.5 V cell potential. a) O_2 recovery (%), b) Molar concentration (%) of CO_2R products (CO, C_2H_4, C_2H_2). See table 1 for cell setup and test operation conditions.

Figure 11 summarizes the outcome of the test conducted to evaluate the effect of the electrolyte temperature on the CO_2 reduction to O_2. As shown in Figure 11a, the O_2 recovery increased substantially, from 0.32 to 12.2 %, as the electrolyte temperature decreased from 22 to 8 degrees Celsius. Two additional species, CO and C_2H_2, besides the expected C_2H_4, were generated, also participating in the O_2 recovery from CO_2, as shown in Figure 11b. C_2H_4 and CO generation at the expense of CO_2 increased at lower electrolyte temperatures, while C_2H_2 decreased as temperature decreased. The beneficial effect of CO_2 on absorption overcomes the negative impact of the reduction in electrolyte electrical conductivity on O_2 recovery at lower temperatures.

B. MFECR Cell Configuration Effect

Two different MFECR cell configurations with the same diameter (11.43 cm) and available active surface area (102.6 cm^2) were used in the preliminary test, as illustrated in Figure 12. In the first configuration shown in Figure 12a, all three flows (CO_2 in the cathode, N_2 in the anode, and KOH solution in the electrolyte) run parallel along a serpentine path. The serpentine wall occupies 30.6 cm^2 and reduces the MFECR's active area from 102.6 cm^2 to 70 cm^2. The second configuration eliminates the serpentine path, as shown in Figure 12b, using all the available active area (102.6 cm^2) in a single wide path.

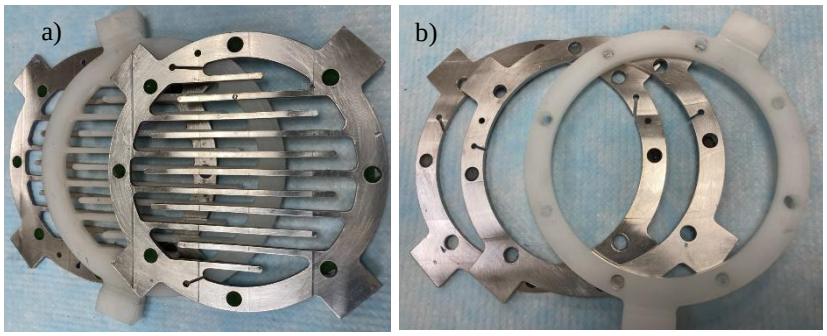

Figure 12. Cell configurations used in the tests. a) with a serpentine b) without serpentine.

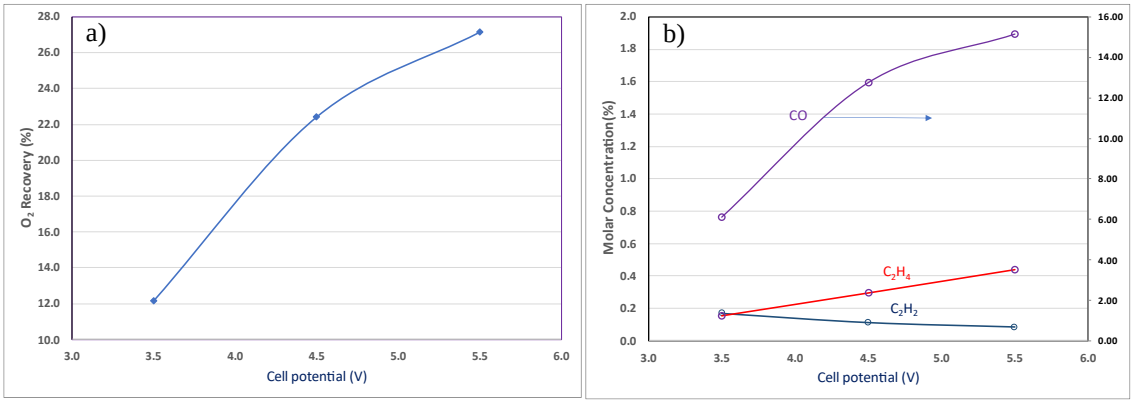

Figure 13. Test outcome for a single cell with serpentine and operation conditions listed in Table 1. a) O_2 recovery, b) CO_2R products (CO, C_2H_4, C_2H_2) at an electrolyte temperature of 8 degrees Celsius.

Figure 13 summarizes the outcome obtained using an MFECR cell with a serpentine path (Figure 12a) leading to an active surface area of 72 cm^2 and conducted under the operation conditions listed in Table 1, keeping the electrolyte temperature at 8 degrees Celsius at different cell potentials from 3.5 to 4.5 and 5.5 V. Both C_2H_4 and CO increased as expected. At the same time, C_2H_2 decreased with the cell potential.

Figure 14 summarizes the outcome obtained using an MFECR cell without a serpentine path (Figure 12b), leading to the use of the entire available active area, 102.6 cm^2, and conducted under the operation conditions listed in Table 2, keeping the electrolyte temperature at 8 degrees Celsius at different cell potentials, from 3.5 to 4.5 and 5.5 V. As in configuration cell with serpentine, C_2H_4 increased as the potential increased. CO, in contrast, decreased as the cell potential increased. C_2H_2, as in the configuration cell with serpentine, also reduced as the cell potential increased.

Cell Type	Without serpentine
GDE	Sigracet 28 BC
GDE type	Modified with carbon black
GDE's cathode	Cu/Br (UTA)
GDE's anode	Platinized Ti (UTA) PTFE/Pt-Ti/Nylon (UTA)
Ionomer on cathode	Fumasep 30 um
Ionomer on anode	None
A(cm^2)	102.58
Electrolyte	1 M KOH solution
CO2 inlet flow (sccm)	50
N2 inlet flow (sccm)	50
Electrolyte inlet flow (mlpl)	100
Potential (V)	3.5, 4.5, and 5.5
Electrolyte temperature (C)	8

Table 2. Electrochemical cell setup without serpentine and operation conditions to evaluate the effect of the cell configuration on the O_2 recovery from CO_2.

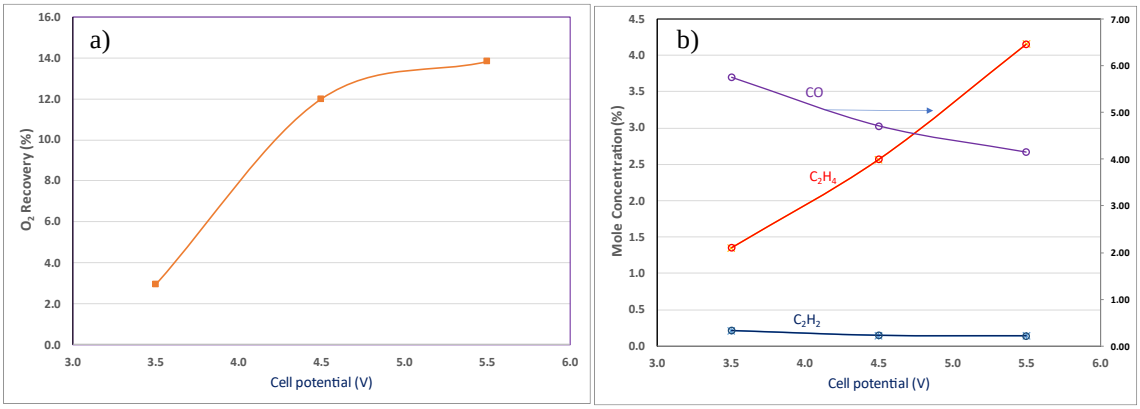

Figure 14. Test outcome for a MFECR cell without serpentine and operation conditions listed in Table 2. a) O_2 recovery, b) CO2R products (CO, C_2H_4, C_2H_2) at an electrolyte temperature of 8 degrees Celsius.

The higher O_2 recovery using the serpentine path (Figure 13a) than without it (Figure 14a), 27% against 14%, is due to the substantial difference in CO generation, 15% against 6.5% at 5.5 V, superseding the higher generation of C_2H_4 observed without serpentine path, 4.1% against 0.4%. A desired trend observed without a sepertine path (Figure 14b) and not with serpentine (Figure 13b) is that the generation of C_2H_4 (the desirable product) increases with potential while the generation of CO decreases. CO is the less desirable product as it reduces O_2 recovery by 50%.

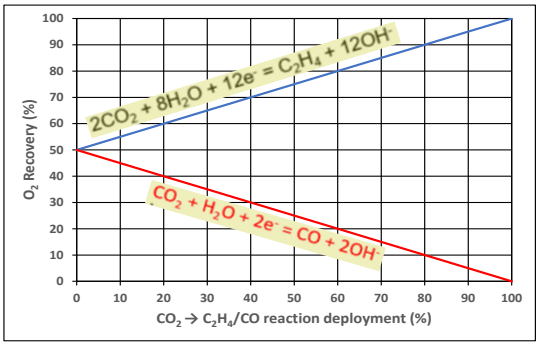

Figure 15. Theoretical O_2 recovery based on the extent of C_2H_4 and CO generation.

As stated above, to achieve a sustainable closed loop on the O_2 recovery from metabolic CO_2, the process needs to generate C_nH_m byproducts with m/n < 2, preferably C_2H_4 or C_2H_2, as their H/C ratios are 2 and 1, respectively. Both MFECR cell configurations yield these two byproducts, with C_2H_4 generated to a much greater extent than C_2H_2 and incremented with the increase of the cell potential. CO is a common competing

byproduct in CO2R, recovering only half of the O_2 in CO_2, as observed in both MFECR cell configurations, reducing the capability of reaching 100% O_2 recovery. Figure 15 illustrates the theoretical O_2 recovery based on the extent of C_2H_4 and CO generation. 100% O_2 recovery will need the CO_2 to be entirely reduced to C_2H_4; if CO_2 is entirely reduced to CO instead of C_2H_4, the O_2 recovery is dropped from 100% to 50%, as illustrated in Figure 15. The ECLSS team at MSFC plans to work further to reduce CO generation at the expense of an increment of C_2H_4 generation to achieve an O_2 recovery of at least 80% that requires, according to Figure 15, the participation of 60% in the generation of C_2H_4 and 40% in the generation of CO.

C. Electrolyte Alternatives

Electrolytes play an essential role in EC CO2R[5,6,7]. Solvents and supporting electrolytes affect the EC processing of CO_2 in several ways. It can influence product distribution and selectivity on the electrocatalyst. The EC window can affect the stability of the electrolyte relative to the applied potential. The conductivity, pH, buffering capacity, CO_2 solubility, and concentration of the cationic and anionic species can influence the electrolytic reduction of CO_2.

The current electrolyte for MFECR is 1M KOH (aq). It provides good conductivity, pH, and material compatibility for the electrodes used in the system. However, KOH poses a spill and corrosion hazard in a spacecraft environment. In addition, it may not provide the optimum medium for CO_2 absorption due to the relatively low solubility of CO_2 in the water solvent at ambient conditions.

The unique physicochemical properties of ionic liquids (ILs) make it a suitable candidate electrolyte for MFECR. ILs are organic salts composed entirely of ions. They exist as liquid below 100 degrees Celsius. They have negligible vapor pressure and generally have high thermal stability[8,9]. ILs are tunable and can be designed to be task-specific by changing the cationic and anionic composition. Some IL ions have a high affinity for CO_2. Thus, the ionic composition of the IL can be designed to improve CO_2 absorption in the electrolyte. In particular, the aprotic heterocyclic anions (AHAs) were known to react with CO_2 reversibly. AHAs are superbase ionic liquids with high CO_2 capacity and solubility attributed to the chemical absorption by the complexation of CO_2 with the anion.

The authors evaluated several ionic liquids, including (AHAs), pyridinium-based, HSO4-based, TFSI-based, triflate-based, and several other ILs already available in the laboratory. Some of these ILs were commercially available, and some were synthesized in-house. A summary of all IL-based electrolytes evaluated for this project is provided in Table 3.

AHA-based	HSO_4-based	TFSI-based	Other ILs
$[P_{44414}][In]$	[BuMePyrr][HSO4]	[BuMePyrr][TFSI]	[EMIm][Ethylsulfate]
$[P_{44414}][BnIm]$	[bmpyrid][HSO4]	[BMIm][TFSI]	$[NHHH_2][NO3]$
$[P_{44414}][4Triz]$	[Emim][HSO4]	[N122(201)][TFSI]	[EMIm][DCA]
$[P_{44414}][CF_3Pyra]$	[mim][HSO4]	[Pmim][TFSI]	[Bmim][$FeCl_4$]
$[EMIm][CF_3Pyra]$	[Pyrro][HSO4]	[Emim][TFSI]	[BuMePyrr][DCA]
$[DABCO][CF_3Pyra]$		[Chol][TFSI]	[BMIm][BF4]
$[P_{44414}][CNPyrr]$	**Triflate-based**	[Bmmim][TFSI]	[EMIm][Oac]
$[P_{44414}][3\text{-}CF_3\ pyra]$	[BuMePyrr][TFO]	$[P_{44414}][TFSI]$	[BMIm][OAc]
$[Emim][4\text{-}CF_3\ im]$	[BMIm][TFO]		$[N(\text{-}2\text{-}OH)_3][SO4m]$
$[memim][3\text{-}CF_3\ pyra]$	[EMIm][TFO]		[Emim][methane sulfonate]
$[P_{66614}][BnIm]$	$[P_{44414}][TFO]$		
	[BMMim][TFO]		

Table 3. Summary of IL-based electrolytes evaluated for MFECR.

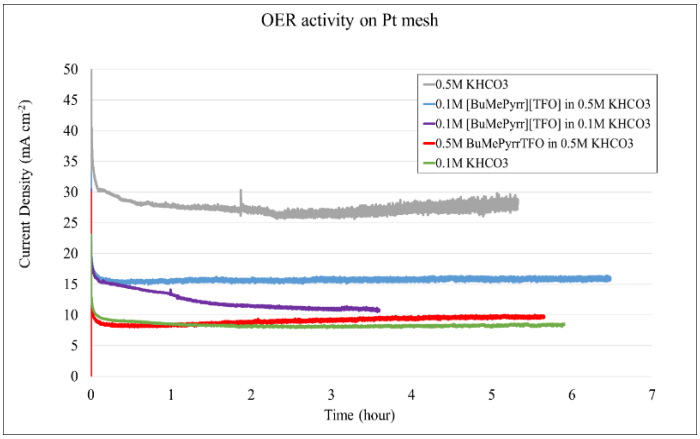

Figure 16. OER activity on Pt mesh anode in aqueous electrolytes.

The IL-based electrolytes were evaluated for water miscibility, copper compatibility, and Nickel foam compatibility. The IL solutions were then evaluated for material compatibility with copper sheet and Nickel foam. Test coupons were prepared by sonicating the copper and Nickel foam coupons in isopropanol and were allowed to dry before testing. Each coupon was immersed in separate solutions for about eight weeks. Observations on the test cell were recorded at 1 hour, one day, eleven days, four weeks, and eight weeks of immersion.

Since [BuMePyrr][TFO] was the most promising candidate in passing the initial requirements (water solubility and electrode compatibility) for alternative electrolytes, it was evaluated for oxygen evolution reaction (OER) activity on Ni foam. Results showed that 1M [BuMePyrr][TFO] (aq) provided a lower current density than 1M KOH (aq). Results also showed degradation of the Nickel foam and electrolyte after electrolysis in 1M [BuMePyrr][TFO] (aq), which changed in color from water-clear to green solution. The color change indicates Nickel oxidation, which is confirmed by the observed dissolution of the electrode. The results demonstrate the instability of Nickel foam for OER in [BuMePyrr][TFO].

[BuMePyrr][TFO] was also evaluated as an additive to the aqueous KHCO3 electrolyte. The mixture was evaluated for OER activity using chronoamperometry, performed using an open and undivided three-electrode EC

cell at room temperature. Ag/AgCl was used as a reference electrode. A high surface area cathode was used as a counter electrode. For this study and the engineering figure of merit for the electrode in the MFECR, the active surface area of the anode was simplified and calculated based on the geometrical surface area of the electrode. Results in Figure 16 showed that [BuMePyrr][TFO] suppressed O_2 formation on Pt mesh in 0.5M KHCO3 (aq). On the other hand, [BuMePyrr][TFO] enhanced O_2 formation on Pt mesh in 0.1M KHCO3 (aq).

IV. Future Work

The outcome of preliminary tests yielded low O_2 recovery for the two MFECR single-cell configurations, 27% (Figure 13) and 14% (Figure 14), using a cell with and without a serpentine path, respectively. This low recovery outcome in a single cell would require an additional cell connected in series to increase the O_2 recovery at the expense of an MFECR size and mass increment. The observed low recovery in a single cell was in part because not only the inlet CO_2 (cathode) and N_2 (anode) flow rates (50 sccm both) were too high, but also the aspect ratio (width: height) of the MFECR serpentine path happened to be too small. A lower inlet flow rate was not possible during the preliminary tests as the GC required a sampling rate of at least 30 sccm. This inlet MFECR flow rate limitation has been overcome for future test runs as the GC sampling rate can now be lower than 30 sccm since a smaller sampling flow is diluted with Argon, carrier gas in the GC.

The MFECR was redesigned and fabricated with a higher aspect ratio of the MFECR serpentine path by reducing its height and keeping the width to enhance the reactant gas exposure with the catalytic surface area underneath the serpentine path. Another significant enhancement has been the in-house fabrication of a new composite-based-GDE cathode replacing the commercially available Sigracet 28BC GDE used in the preliminary tests; the catalyst is deposited throughout the in-house GDE and not only on the CL of the Sigracet 28BC GDE to increase the catalysis surface area in a single cell with the same available MFECR's active surface.

The effect of the electrolyte alkalinity on the faradaic efficiency onsets of C_2H_4 and CO will be assessed, as reduction of these onsets is reduced as the alkalinity of the KOH electrolysis solution increases[10]. The increment of alkalinity also decreases the freezing temperature of the KOH solution, allowing lower electrolyte inlet temperature that leads to a significant increment of O_2 recovery, as observed in the preliminary tests. During the alkalinity assessment, lower temperature operation will also be attempted to evaluate the temperature driven O_2 recovery.

A. MFECR redesign

A comprehensive digital twin (replica) of the MFECR has been built in-house using a rigorous 3D model to conduct qualitative model-based analysis to evaluate proposed design upgrades and enhance/optimize the O_2 recovery in a single cell[4]. The MFECR's digital twin assessed an increment in the MFECR aspect ratio of the serpentine path of all three chambers (cathode, anode, and electrolyte). Two path wall heights were evaluated, the current one, 3.2 mm, and a half-reduced one, 1.6 mm, keeping the same width, 4 mm, increasing the MFECR's path aspect ratio from 1.25 to 2.5 and using the same inlet pure CO_2 inlet flow rate in both path aspect ratios and width (4 mm) as well as length (900 mm) of the serpentine path. Figure 17 summarizes the outlet composition in both assessment cases, 3.2- and 1,6-mm path height, respectively; the C_2H_4 outlet composition substantially increases as the aspect ratio rises from 1.5 (3.6 mm height) to 2.5 (1.6 mm height).

As illustrated in Figure 17, the digital-twin-based assessment indicates that reducing the serpentine-path height of the serpentine path of the MFECR used in these preliminary tests (3.2 mm) to 1.6 mm leads to the increment of the C_2H_4 generation (and the O_2 recovery). The MFECR used in the preliminary tests has been upgraded with a serpentine path height of 1.6 mm and is expected to be used in future tests. Two upgraded MFECRs were fabricated, with 1.6 mm serpentine height but with different numbers of paths, one with 12 as the MFECR used in the preliminary tests and the other with four wider paths. The outcome of the initial tests indicates that a wider path favors the formation of C_2H_4 at the expense of CO at higher potentials, as stated and illustrated above when two tests were run at the same conditions but one with 12 paths and the other with a single path (Figure 13b and 14b).

Figure 18 illustrates the initial and the two upgraded MFECRs and their respective anode, cathode, and electrolyte chambers. The images labeled as a) correspond to the MFECR used in the preliminary tests conducted so far and reposted in this paper; the images labeled as b) and c) correspond to two MFECRs with the same upgraded aspect ratio from 1.25 to 2.5 (decrement of the serpentine height from 3.2 to 1.6 mm) but a different number of serpentine paths, 12 and 4 respectively. The cathode and the anode serpentine chambers of the upgraded MFECR (b and c) differ from the initial MFECR cathode and anode serpentine chambers (a), not only in the serpentine path height but also in the material type; the upgraded ones are made of Teflon to mitigate the formation of Potassium carbonate when Nickel foam electrode is used, as observed in Figure 8. The electrolyte will be in contact with Teflon instead of Nickel, avoiding the potential catalytic participation of Nickel in the formation and precipitation of Potassium carbonate. The upgraded MFECR cell shown in the second column in Figure 18 will be used in future tests.

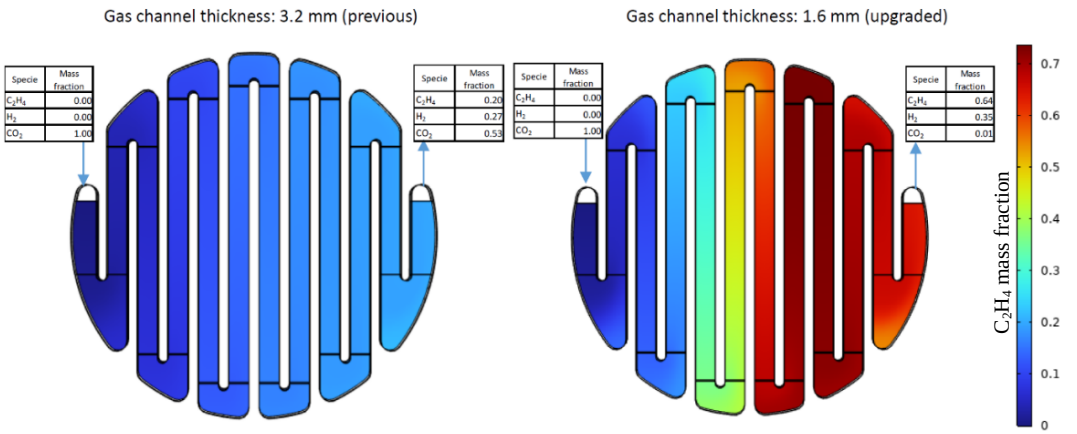

Figure 17. C_2H_4 mass fraction profile in both modeled-based study cases, 3.2- and 1.6-mm serpentine-wall height, respectively.

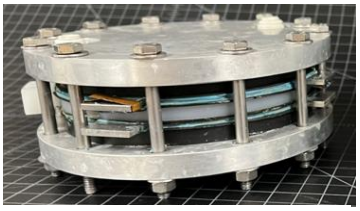

a) Initial MFECR with 1.6 mm serpentine wall and 12 paths.

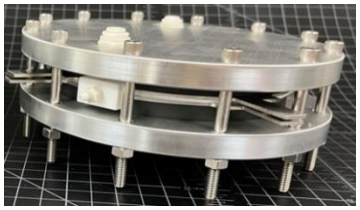

b) Upgraded MFECR with 1.6 mm serpentine wall and 12 paths.

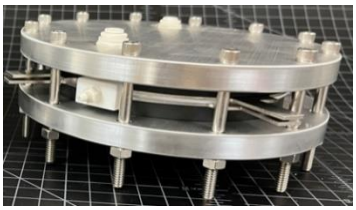

c) Upgraded MFECR with 1.6 mm serpentine wall and 4 paths.

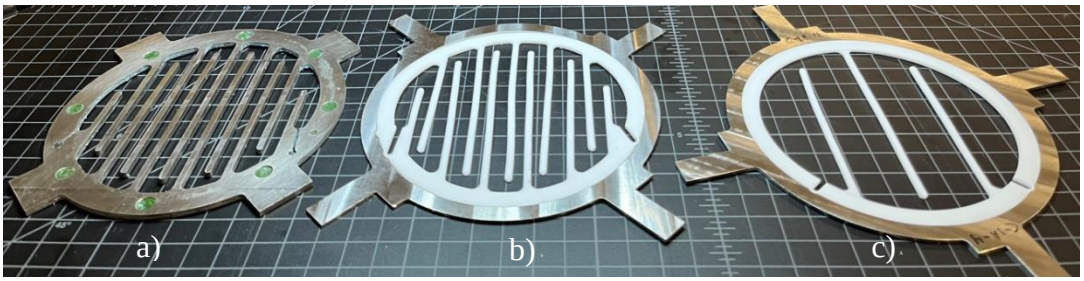

Anode serpentine chamber

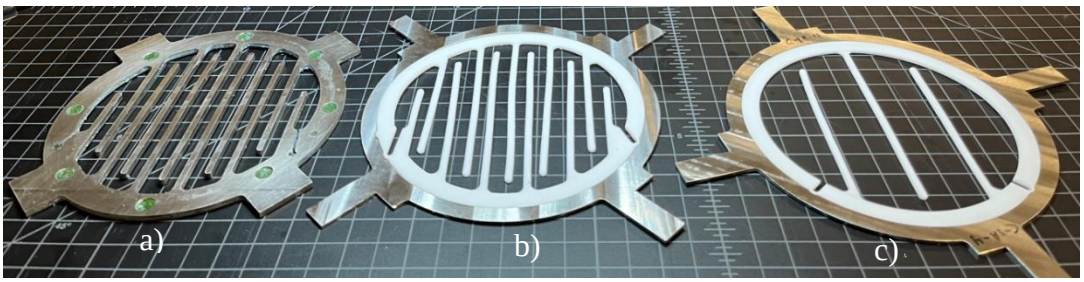

Cathode serpentine chamber

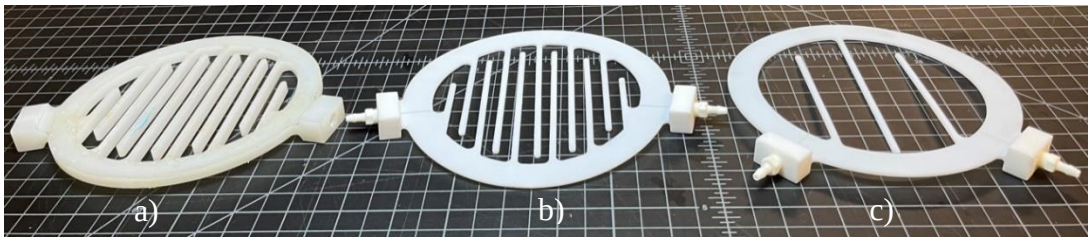

Electrolyte serpentine chamber

Figure 18. Initial and upgraded MFECR cells with 3.6- and 1.6-mm serpentine path height respectively.

B. Fabrication and Use of a Cathode Composite

In the commercially available cathode GDE (Sigracet 28 BC) used in the preliminary tests, the Cu-Br catalyst is housed on the MPL of the GDE, forming the CL throughout the GDE's outer surface, as illustrated in Figure 19a. A cathode composite has been fabricated in-house to increase the catalyst density and surface area using a similar setup used in the anode, A Nylon membrane in contact with the electrolyte, a PTFE film in contact with the CO_2 gas, and GDE without MPL (Sigracet 39AA). The Cu-Br catalyst is housed throughout the entire volume of the GDE and not just the GDE outer surface (CL), as in the case of the GDE used in the preliminary tests. This in-house GDE with enhanced catalyst density has been fabricated and can be used in future tests.

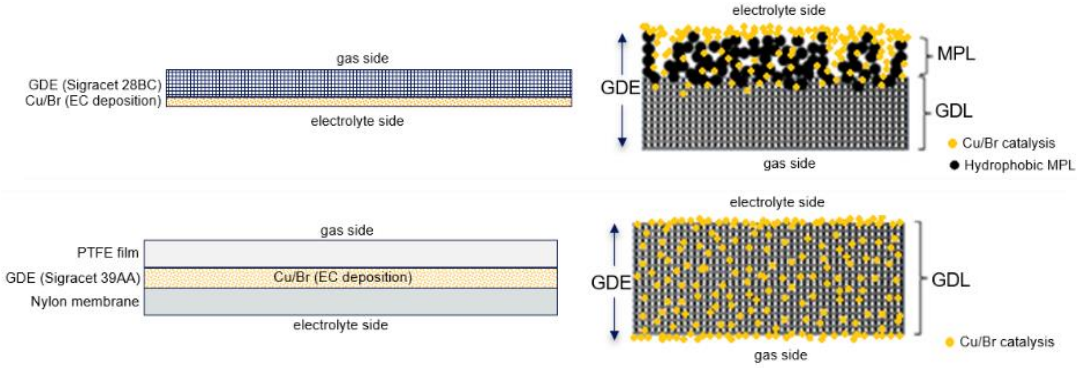

Figure 19. a) Cathode GDE used in preliminary tests, b) Redesigned composite cathode fabricated in-house to increase catalyst surface density.

C. Electrolyte alternatives and KOH alkalinity

As stated above, several ILs were investigated for EC evaluation, and none have been selected as a feasible alternative to KOH as the best prospect candidate [BuMePyrr][TFO] provided a lower current density than KOH and an instability with the Nickel foam for OER.

Alternative K substitution in the KOH includes Li, Na, Rb, and Cs, all four with the same cation charge value (+1) but different sizes, Li being the smallest (69 pm) and Cs the largest (170 mp). The cation size of the electrolyte is known to affect the EC reduction of CO_2 over metal; however, a satisfactory explanation for this phenomenon has not been developed. A previously unrecognized consequence of cation hydrolysis near the cathode might explain this phenomenon[11]. With increasing cation size, the acid-ionization constant (pKa) decreases and is sufficiently low for hydrated K+, Rb+, and Cs+ to serve as buffering agents, lowering the pH near the cathode, leading to an increase in the local concentration of dissolved CO_2 and an increase of cathode activity. A benchmark of three hydroxides, KOH, LiOH (with the lightest cation), and CsOH (with the largest cation), will be evaluated in future tests.

In the CO_2 reduction reaction, the faradaic onset potential gap between CO and C_2H_4 is attributed to the need to build up coverage of surface-adsorbed CO (*CO) across the catalyst surface before CO dimerization becomes energetically favorable. As the electrolyte pH increases, the penetration distance of CO_2 into the electrolyte is notably diminished through direct interaction with hydroxide molecules[12]. C_2H_4 and CO faradaic efficiencies have shown a reduction of C_2H_4 onset potential with increasing KOH concentration[13]. In all preliminary tests, the KOH concentration was 1 M; the effect of higher KOH concentration on the faradaic efficiency onsets of C_2H_4 and CO will be evaluated in future tests.

D. H_2 separation from the cathode outlet stream

As illustrated in Figures 5a and 5c, the outlet stream of the cathode cell chamber carries C_2H_4 and CO (from CO_2 reduction, equations 5 and 6), H_2 (from water electrolysis, equation 7), and unreacted CO_2. In parallel, the outlet stream of the anode cell chamber carries O_2 from two sources: CO_2 reduction and water electrolysis. H_2 separation from C_2H_4, CO, and CO_2 is required either to use it as a final product or to recover the electrolyte water by feeding the separated H_2 and the O_2 stream to a fuel cell. Figure 20, taken from Figure 5c, shows a general schematic of the H_2 separator coupled with a fuel cell to recover the water consumed in the MFECR during the electrolysis of water in the electrolyte.

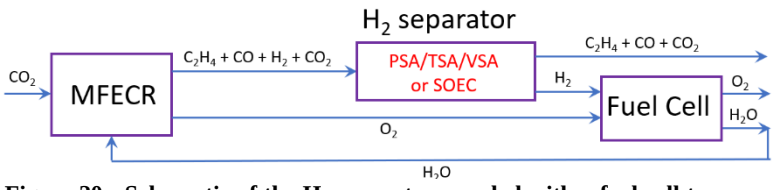

Figure 20. Schematic of the H_2 separator coupled with a fuel cell to recover the water consumed in the MFECR.

Two H_2 separation approaches will be evaluated: Pressure/Temperature/Vacuum Swing Adsorption (PSA/TSA/VSA) and proton transfer using a solid oxide electrochemical cell (SOEC) equipped with an in-housed-fabricated ceramic membrane. Adsorption breakthroughs conducted on zeolite 13X and activated carbon (AC) confirmed the selective adsorption of C_2H_4, CO, and CO_2, not H_2 on 13X and AC. A pilot PSA/VSA/TSA unit was designed and fabricated to be used in future tests. A second approach will use a Yttria-doped Barium Zirconate (BZY) ceramic membrane to selectively transfer H_2 in the form of $2H^+$ (protons) throughout the membrane under an electrical potential applied on both sides. BZY is an efficient proton(H^+)-conducting membrane manufactured in-house using a proprietary solid-state reactive sintering (SSRS) method.

Acknowledgment

We especially thank our colleagues West Kelly and Kenneth Bodki at NASA Marshall Space Flight Center for her valuable participation and contribution to this project, from origination and redesign to startup and daily operation. We owe them great gratitude for their unrestricted support of this project.

References

[1] Brown B. R., Curreri P. A., Rabenberg E. M., Dominguez J. A., Reidy L. P., Dennis B., Chanmanee W., Burke K. A., Developmental efforts of an electrochemical oxygen recovery system for advanced life support, International Conference on Environmental Systems (ICES), 50th International Conference on Environmental Systems, paper 74, pp. 11-12.

[2] Tacconi N. S., Chanmanee W., Dennis B., Rajeshwar K., Continuous flow reactor and hybrid electrocatalyst for high selectivity production of C_2H_4 from CO_2 and water via electrolysis, patent US11299811B2 granted 2022-04-12.

[3] Dominguez J., Reidy L., Crawford K., Oliver-Butler K., Black C., Brown B., Dennis B., Chanmanee W., McCall S., Burke K., Development of an efficient alternative to recovery O_2 from metabolic CO_2 via electrolysis operated at ambient temperature and driven by highly selective catalysis, International Conference on Environmental Systems (ICES), 52nd International Conference on Environmental Systems, July 2023. Calgary, Canada.

[4] Dominguez J., Reidy L., Crawford K., Oliver-Butler K., Black C., Brown B., Dennis B., Chanmanee W., McCall S., Burke K., Comprehensive 3D Multiphysics Model on Electrochemical Recovery of O_2 from Metabolic CO_2 at the International Space Station (ISS), International Conference on Environmental Systems (ICES), 52rd International Conference on Environmental Systems, July 2023. Calgary, Canada

[5] Zheng, Y., et al. 2019. Understanding the Roadmap for Electrochemical Reduction of CO_2 to Multi-Carbon Oxygenates and Hydrocarbons on Copper-Based Catalysts. J. Am. Chem. Soc. 141, 7646−7659

[6] Pupo, M., and Kortlever, R. 2019. Electrolyte Effects on the Electrochemical Reduction of CO_2. Chem. Phys. Chem 20 (22), 2926– 2935

[7] Konig, M., Vaes, J., Klemm, E., and Pant, D. 2019. Solvents and Supporting Electrolytes in the Electrocatalytic Reduction of CO_2. iScience 19, 135–160

[8] Fillion, J. J.; Xia, H.; Desilva, M. A.; Quiroz-Guzman, M.; Brennecke, J. F. 2016. Phase Transitions, Decomposition Temperature, Viscosities, and Densities of Phosphonium, Ammonium, and Imidazolium Ionic Liquids with Aprotic Heterocyclic Anions. J. Chem. Eng. Data. 61,8, 2897-2914

[9] Plechkova, N. V.; Seddon, K. R. 2008. Applications of ionic liquids in the chemical industry. Chem. Soc. Rev. 37, 123−150

[10] Dinh C., Burdyny T., Kibria M. G., Seifitokaldani A., Gabardo C. M., García A., Kiani A., Edwards J. Luna P. D., Bushuyev O. S., Zou C., Quintero-Bermudez R., Pang Y, Sinton D., Sargent E. H. CO_2 electroreduction to ethylene via hydroxide-mediated copper catalysis at an abrupt interface. 2018. Science 360, 783–787.

[11] Singh M. R., Kwon Y., Lum Y., Ager J. W., Bell A. T. Hydrolysis of Electrolyte Cations Enhances the Electrochemical Reduction of CO_2 over Ag and Cu. J. Am. Chem. Soc. 2016, 138, 13006−13012.

[12] N. Gupta, M. Gattrell, B. MacDougall, J. Appl. Electrochem. 36, 161–172 (2006).

[13] Dinh, C. T., Burdyny, Kibria G., Seifitokaldani, A., Gabardo C. M., García de Arquer P., Kiani A., Edwards J. P., De Luna, P., Bushuyev O. S., Zou C.,1, Quintero-Bermudez R., Pang, Y., Sinton D., Sargent E. H. CO_2 electroreduction to ethylene via hydroxide-mediated copper catalysis at an abrupt interface. Science 360, 783–787 (2018)